J. Phys.: Condens. Matter **20** (2008) 064228 (14pp) doi:10.1088/0953-8984/20/6/064228

Discovery of novel hydrogen storage materials: an atomic scale computational approach

C Wolverton[1], Donald J Siegel[2], A R Akbarzadeh[3] and V Ozoliņš[3]

[1] Department of Materials Science and Engineering, Northwestern University, Evanston, IL 60208, USA
[2] Ford Research and Advanced Engineering, RIC/MD 1170, Dearborn, MI 48121, USA
[3] Department of Materials Science and Engineering, University of California, Los Angeles, CA 90095-1595, USA

Received 4 September 2007, in final form 29 October 2007
Published 24 January 2008
Online at stacks.iop.org/JPhysCM/20/064228

Abstract

Practical hydrogen storage for mobile applications requires materials that exhibit high hydrogen densities, low decomposition temperatures, and fast kinetics for absorption and desorption. Unfortunately, no reversible materials are currently known that possess all of these attributes. Here we present an overview of our recent efforts aimed at developing a first-principles computational approach to the discovery of novel hydrogen storage materials. Such an approach requires several key capabilities to be effective: (i) accurate prediction of decomposition thermodynamics, (ii) prediction of crystal structures for unknown hydrides, and (iii) prediction of preferred decomposition pathways. We present examples that illustrate each of these three capabilities: (i) prediction of hydriding enthalpies and free energies across a wide range of hydride materials, (ii) prediction of low energy crystal structures for complex hydrides (such as $Ca(AlH_4)_2$ $CaAlH_5$, and Li_2NH), and (iii) predicted decomposition pathways for $Li_4BN_3H_{10}$ and destabilized systems based on combinations of $LiBH_4$, $Ca(BH_4)_2$ and metal hydrides. For the destabilized systems, we propose a set of thermodynamic guidelines to help identify thermodynamically viable reactions. These capabilities have led to the prediction of several novel high density hydrogen storage materials and reactions.

(Some figures in this article are in colour only in the electronic version)

1. Introduction

Vehicles utilizing hydrogen as a fuel are reliant on an efficient means of storing hydrogen on board the vehicle. Currently available technologies fall far short of targeted storage densities, both by volume and by weight (Satyapal *et al* 2007). In addition to density, the thermodynamics of inserting and releasing hydrogen from a storage material are also critical, as they dictate limits on the temperatures/pressures at which these defueling/refueling reactions can occur. On-board vehicle applications place bounds on the practical operating conditions of such a hydrogen storage system, and therefore provide bounds on the thermodynamics and kinetics that are suitable. Thus, there is currently a global effort aimed at developing a material which will store hydrogen at a high gravimetric and volumetric density, and which will allow rapid, energy efficient (de)hydriding reactions at near-ambient conditions (Satyapal *et al* 2007).

A purely Edisonian experimental approach to discovery of novel storage materials via synthesis and characterization is time-consuming and inefficient due to the numerous possible reaction pathways, (often) slow reaction kinetics, as well as the sheer number of possible novel compositions. One approach to improve on this purely empirical search would be an accurate, physics-based modeling approach that yields the thermodynamic functions of reactants and products and hence hydrogen desorption reaction enthalpies. We describe such an approach here. This type of computational screening can accelerate the discovery of novel crystal structures, reaction pathways, and material compositions for optimized storage performance.

A viable computational approach to the discovery of new hydrogen storage materials is immediately faced with several

significant challenges: (1) *Demonstration of quantitatively accurate reaction energies*: the computations must provide an accurate picture of the thermodynamics of (de)hydriding reactions so that one can confidently differentiate promising reactions from thermodynamic 'dead ends'. (2) *Prediction of hydride crystal structures*: this challenge is highly non-trivial, as one could argue that the *a priori* prediction of crystal structure is one of the most basic fundamental, unsolved problems in condensed matter physics, solid-state chemistry, and materials science. (3) *Prediction of hydride decomposition pathways*: this often overlooked challenge is also key. The novel hydride material will, at best, only give the *reactants* of a new hydrogen storage reaction; determining the thermodynamically preferred desorption *products* for new storage reactions can involve complex, highly non-intuitive pathways, as we show below.

In this article, we review a computational approach based on first-principles density-functional theory (DFT) calculations aimed at discovery of novel hydrogen storage materials and reactions. Specifically, we describe our efforts at overcoming the above three key challenges in constructing such an approach, and demonstrate how DFT calculations can provide a key tool in the arena of materials discovery.

2. First-principles methodology

Our electronic-structure total energy calculations are based on density-functional theory (DFT), (Hohenberg and Kohn 1964, Kohn and Sham 1965) as implemented in the highly efficient VASP code (Kresse and Hafner 1993, Kresse 1993, Kresse and Furthmüller 1996a, 1996b). Core–electron interactions are described by either ultrasoft pseudopotentials, (Vanderbilt 1990, Kresse and Hafner 1994) or projector augmented wave (PAW) potentials (Blöchl 1994). For exchange–correlation, we use the generalized gradient approximation (GGA) of Perdew and Wang (Perdew and Wang 1992) as we have previously (Wolverton *et al* 2004) shown the GGA to be generally superior to the local density approximation for calculating the thermodynamic properties of hydrogen storage materials. We optimize all atomic positions, cell shape, and cell volume. Vibrational spectra were obtained using the frozen phonon technique (Wei and Chou 1992). Each symmetry-inequivalent atom was displaced along all symmetry-inequivalent directions and forces on all atoms were calculated to obtain a row of the dynamical matrix. Other details of the calculations have been given previously (Wolverton *et al* 2004, Wolverton and Ozoliņš 2007, Ozoliņš *et al* 2007, Magyari-Kope *et al* 2006, Siegel *et al* 2007a, 2007b, Akbarzadeh *et al* 2007).

3. Accuracy of DFT for hydrogenation enthalpies

Density-functional theory (DFT) has become a *de facto* standard tool for computing the crystal binding energies of complicated crystalline materials. However, because the hydrogen release reactions involve H_2 as the final product, and most of the current DFT functionals are known to perform worse for molecules and atoms than for extended systems, it is legitimate to ask whether the calculated DFT formation energies are accurate enough to screen for useful hydrogen storage materials. In other words one needs to have a quantitative understanding of the accuracy of DFT predicted thermodynamics to evaluate the usefulness of the DFT for predicting metal hydride hydrogen storage thermodynamics. Previously, we have performed a thorough study of the $T = 0$ K static energetics for a large number of hydride compounds (Wolverton *et al* 2004). In that study, we found that for most compounds the hydrogen release enthalpies were predicted with a typical accuracy of ∼10–20 kJ/mol H_2 using the generalized gradient approximation (GGA) to the exchange–correlation functional. We also found that the local density approximation (LDA) systematically yielded higher hydrogenation enthalpies than the GGA, which we attributed to the GGA/LDA difference in the description of the H_2 molecule. In that same study, we went beyond the $T = 0$ static energies for one specific compound, AlH_3, and computed the finite temperature thermodynamics associated with release of H_2 from this hydride. These finite temperature properties are computed from the contributions due to vibrational free energies on the storage thermodynamics. More recently, we have used this more complete static + dynamic approach to compute the thermodynamics of storage reactions, across a wide variety of reaction types (Wolverton and Ozoliņš 2007, Ozoliņš *et al* 2007, Magyari-Kope *et al* 2006, Siegel *et al* 2007a, 2007b, Akbarzadeh *et al* 2007). This first-principles approach has resulted in calculated thermodynamic properties which agree well with experimental measurements. We also note another very recent study of the accuracy of DFT for hydride reactions by Hector *et al* (Hector *et al* 2007).

Here we demonstrate the accuracy of DFT for hydride reactions by showing the calculated thermodynamic properties of dehydrogenation reactions for simple binary hydrides of the alkali, alkaline earth, and early transition metals, collectively denoted by M. In spite of the limited practical usefulness of these reactions for hydrogen storage, it is useful to carefully evaluate the enthalpies and entropies of these reactions to validate the accuracy of the current first-principles electron-structure techniques. These metal hydrides decompose according to the following generic reaction[4]:

$$\mathrm{MH}_n \rightarrow \mathrm{M} + n/2\mathrm{H}_2. \tag{1}$$

The enthalpy corresponding to equation (1) can be expressed as

$$\Delta H = \frac{n}{2}\left[E_{\mathrm{tot}}^{\mathrm{H}_2} + E_{\mathrm{vib}}^{\mathrm{H}_2}(T) + \frac{7}{2}k_{\mathrm{B}}T\right] + E_{\mathrm{tot}}^{\mathrm{M}}(T) + E_{\mathrm{vib}}^{\mathrm{M}}(T) - E_{\mathrm{tot}}^{\mathrm{MH_n}}(T) - E_{\mathrm{vib}}^{\mathrm{MH}_n}(T), \tag{2}$$

where E_{tot} is the static DFT total energy and E_{vib} is the vibrational energy obtained from first-principles calculated phonon frequencies, including the zero-point vibrations.

[4] Some metal hydrides decompose in a more complex manner than equation (1), e.g., VH_2 and PdH go through a series of different metal-to-H stoichiometries. To ensure that our results are comparable for different regions of the periodic table, we only consider the ideal decomposition equations that can be written as equation (1). For instance, the energetics of VH_2 given in figure 1 are for decomposition into $V + H_2$.

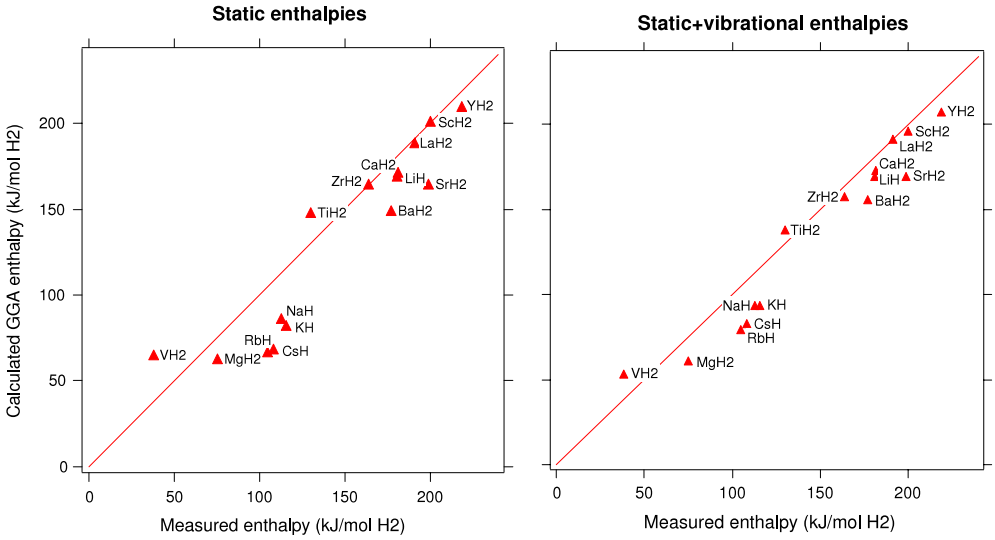

Figure 1. Calculated versus measured $T = 298$ K dehydrogenation enthalpies for a series of metal hydrides. Calculated values were obtained using the Perdew–Wang GGA. Values in the right panel include vibrational effects. Experimental values are taken from Manchester (2000); see also Wolverton *et al* (2004).

Our results for the hydrogen desorption enthalpies are shown in figure 1 as a diagonal plot of the calculated versus measured enthalpies. To illustrate the effect of dynamical contributions to the enthalpy, we show plots of calculated values without and with vibrational energies. Overall, we find that the GGA reproduces the measured enthalpies rather well, especially if the vibrational contributions are included. The average rms error decreases from 19.4 to 14.7 kJ/mol H_2 when vibrational effects are included, while the maximum errors undergo a more pronounced reduction: the largest underestimate of the dehydriding enthalpy goes down from 39 kJ/mol H_2 in CsH to 29.3 kJ/mol H_2 in SrH_2; the largest overestimate goes from -27 to -15 kJ/mol H_2 in VH_2. Only in a few isolated cases (MgH_2, YH_2 and ZrH_2) are the errors increased by a small amount (a few kJ/mol H_2) by including the vibrational effects. We conclude that vibrations can significantly improve the predictive accuracy of the Perdew–Wang GGA and should therefore be included in state-of-the-art studies of hydrogen storage materials.

4. Prediction of hydride crystal structures

We next move to the second computational challenge: predicting hydride crystal structures. In order to predict the energetics of the decomposition of H_2 storage compounds, one first has to know the energy, and hence the crystal structure of these phases. For compounds which have yet to be synthesized, the crystal structures will not be known experimentally; hence a key capability for any atomistic computational approach involves the prediction of low energy crystal structures. We illustrate several different approaches to this problem of crystal structure prediction. We note that we do not discuss here several new, promising techniques (e.g., genetic algorithm methods (Glass *et al* 2006), Monte Carlo optimization methods (Ozoliņš *et al* 2007), etc) directed towards solving this problem.

4.1. Database (ICSD) searching methods

The first approach involves searching for structural candidates from crystallographic databases, such as the International Crystal Structures Database (ICSD) (Hellenbrandt 2004). The idea is straightforward: first, one constructs a set of candidate crystal structures from the ICSD (or other) database using structures of chemically similar compounds. Next DFT calculations are performed on each of the candidate structure types to identify the lowest energy structure. For the lowest energy structure(s), one then computes phonons and verifies the dynamic stability of the structure. If the compound is dynamically unstable, one may either displace atoms along the unstable mode(s) and re-relax, or perform DFT-based molecular dynamics simulations to search for lower energy geometries. For relatively simple stoichiometries and common chemistries, one can often find a relatively large set of candidate structures ($\sim$100), which provides a large pool to sample the configuration space of crystal structure types. This database searching approach has recently become quite popular in the study of hydride crystal structures (e.g., see Vajeeston *et al* 2004, Løvvik and Swang 2004, Ke *et al* 2005, Ozoliņš *et al* 2007, Wolverton and Ozoliņš 2007), but has also been used to identify unsuspected low energy structures in intermetallic systems (Zhong *et al* 2004) and other materials classes.

While we have utilized this approach to investigate the crystal structure of a wide variety of alanates and borohydrides (see, e.g., Wolverton and Ozoliņš 2007, Ozoliņš *et al* 2007), here we focus on the storage reactions involving calcium alanate. (A more detailed description of these results is given in Wolverton and Ozoliņš 2007.) Calcium alanate, $Ca(AlH_4)_2$, and its decomposition products have recently been synthesized and studied using x-ray diffraction (XRD), NMR and IR spectroscopies, and differential scanning calorimetry (DSC) (Mamatha *et al* 2006, Fichtner *et al* 2005). The proposed three-

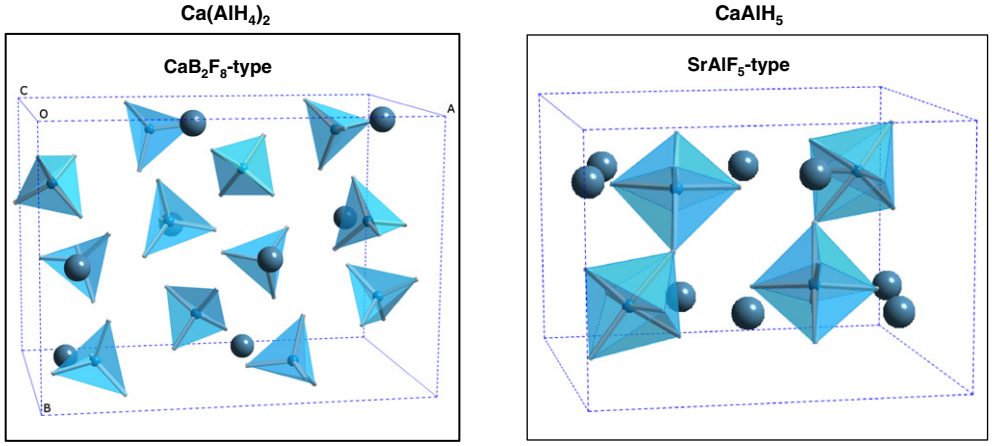

Figure 2. DFT predicted crystal structures of $Ca(AlH_4)_2$ and $CaAlH_5$. Using a database searching method, these structures were the lowest energy structures found out of a set of ∼200 candidate structure types (Wolverton and Ozoliņš 2007).

step decomposition sequence is:

$$Ca(AlH_4)_2 \rightarrow CaAlH_5 + Al + \tfrac{3}{2}H_2 \rightarrow CaH_2 + 2Al + 3H_2 \rightarrow CaAl_2 + 4H_2.$$

DSC measurements indicate the enthalpies of the first and second steps are slightly exothermic (−7 kJ/mol H_2) and endothermic (+32 kJ/mol H_2), respectively (Mamatha *et al* 2006).

The crystal structure of $Ca(AlH_4)_2$ is experimentally unknown, and $CaAlH_5$ has only recently (Weidenthaler *et al* 2006) been determined. To search for these structures computationally, we have used a large database of candidate AB_2C_8 and ABC_5 crystal structure types: from the ICSD, we find a set of candidate crystal structures for compounds of stoichiometry AB_2C_8 and ABC_5 where C = H/D, F, Cl, S, Br, Te, I, and O. In total, we construct a set of *93 candidate AB_2C_8 structures* and *84 candidate ABC_5 structures*. For $Ca(AlH_4)_2$, we find that the lowest energy structure out of the 93 structure types we explored is the CaB_2F_8-type structure (figure 2). This prediction is in agreement with other DFT calculations (Løvvik 2005) and is awaiting experimental confirmation. In addition, we uncover several phases (e.g., β-$ThMo_2O_8$-type, $AgAu_2F_8$-type, and $PbRe_2O_8$-type) very competitive in energy with the ground state structure. For $CaAlH_5$, we find the stable structure type to be the α'-$SrAlF_5$-type, in agreement with recent observations. Again, we find structures close in energy to the ground state: $UTlF_5$-type, $SrFeF_5$-type and $BaGaF_2$-type.

For the low energy $T = 0$ K phases, we perform DFT frozen phonon calculations to ascertain the zero-point and vibrational entropy contributions to the thermodynamics of decomposition. We generally find agreement with recent experiments, and our calculations show that the three-step decomposition of $Ca(AlH_4)_2$ is divided into a weakly exothermic first step, a mildly endothermic second step, and a strongly endothermic third step (−9, +23, and +72 kJ/mol H_2 at $T = 300$ K). The excellent agreement between observations and computation for both crystal structures and thermodynamic properties gives one confidence in the utility of this database searching approach.

4.2. Lattice algebra enumeration

The database searching method discussed above has been quite effective in a number of applications, but has the serious restriction that it is incapable of predicting completely new, unobserved crystal structure types. We next describe a method that does not face this restriction: lattice algebra enumeration (Magyari-Kope *et al* 2006). We illustrate this method in the search for the structure of the hydrogen storage material, Li_2NH.

The crystal structure of lithium imide, Li_2NH, has prompted several recent studies. All experimental investigations consistently point to a room temperature structure with Li and N ions occupying the positions of an antifluorite structure. However, there are conflicting reports on the H positions. Some reports suggested that hydrogen is distributed in a disordered manner across various Wyckoff positions within the fluorite framework (Juza and Opp 1951, Noritake *et al* 2005, Ohoyama *et al* 2005). On the other hand, recent studies by Herbst and Hector (2005) and Balogh *et al* (2006) have deduced a lower symmetry, ordered arrangement of H positions of orthorhombic *Ima*2 symmetry. Our DFT-driven search method allows a systematic enumeration of possible configurations of H atoms and yields several low energy ordered arrangements based on the antifluorite structure (Magyari-Kope *et al* 2006). The method is made possible by noting that this ordering problem may be mapped onto a binary alloy problem, which allows us to utilize well-established lattice algebra methods developed in the alloy theory community. We consider (small unit cell) input structures where all N–H dimers are aligned either parallel or antiparallel to one of several principle orientations. For a given orientational axis, the problem of listing different N–H dimer arrangements can be viewed as formally identical to the binary alloy problem on a fixed fcc lattice: by placing Li and N atoms in cubic fluorite structural positions, N forms a fcc sublattice. We then associate parallel N–H alignments with 'atoms' of type A and antiparallel H–N alignments with atoms of type B. Although this is a considerable simplification, there is still an astronomical number 2^N where N is the number of sites of possible ordered structures for this

Table 1. Formation energies of $Li_4BN_3H_{10}$ in units of kJ/(mol $Li_4BN_3H_{10}$). ΔE represents the static $T = 0$ K DFT energy; $\Delta H^{T=300\text{ K}}$ includes zero-point energies and adds finite temperature vibrational and molecular (rotational + translational + pV) energies. The free energy of formation at $T = 300$ K, $\Delta G^{T=300\text{ K}}$, adds vibrational (solids) and tabulated (molecular) entropies to $\Delta H^{T=300\text{ K}}$.

	Reaction	ΔE	$\Delta H^{T=300\text{ K}}$	$\Delta G^{T=300\text{ K}}$
(a)	$4Li + B + 3/2N_2 + 5H_2 \rightarrow Li_4BN_3H_{10}$	−806.9	−708.1	−454.6
(b)	$3LiNH_2 + LiBH_4 \rightarrow Li_4BN_3H_{10}$	−11.3	−11.8	−10.2

configurational problem. However, using lattice algebra methods developed in the field of alloy theory (Ozoliņš *et al* 1998), we can enumerate all possible ordered arrangements based on this lattice type, up to a specified cell size.

By scanning through a large number of ordered arrangements, we find a low energy structure of Li_2NH that has orthorhombic *Pnma* symmetry at $T = 0$ K. Perhaps more importantly, we note it is lower in energy than *all* of the previously proposed structures based on diffraction experiments. Using our predicted structure, we have calculated the enthalpy of the reaction:

$$LiNH_2 + LiH \rightarrow Li_2NH + H_2.$$

Including the vibrational energy and entropy contributions we find an enthalpy of 63.7 kJ/mol H_2 at $T = 0$ K, and 74.8 kJ/mol H_2 at $T = 300$ K, which compares favorably with the experimental values of 64–66 kJ/mol H_2 (Chen *et al* 2002, Kojima and Kawai 2005). This agreement gives us confidence in the utility and predictive power of this method. We also note that subsequent to our work, Mueller and Ceder (2006) have extended this type of approach via another alloy theory method, the cluster expansion (Ozoliņš *et al* 1998), and have predicted an even lower energy structure. These types of studies demonstrate that this method is capable of predicting new, unsuspected ground state structures.

5. Predicting reaction pathways

The reaction pathway by which a hydrogen storage material will absorb or release hydrogen will depend upon the kinetic and thermodynamic properties of the system. In equilibrium, and at a specified temperature and pressure, the phases present during the (de)hydriding process will be those which minimize the free energy of the system in contact with a gas-phase reservoir of hydrogen. Knowledge of these phases is essential, as quantifying their relative proportions is a mandatory precondition for the subsequent prediction of the enthalpy of reaction, ΔH.

The prediction of realistic reaction pathways is thus our third prerequisite for a predictive computational approach capable of screening potential hydrogen storage reactions based on their enthalpies. In our prior work (Siegel *et al* 2007a, Akbarzadeh *et al* 2007), we have utilized two approaches to address this reaction pathway issue: (i) pathway enumeration (Siegel *et al* 2007a) and (ii) the development of an automated tool for the prediction of all thermodynamically feasible reactions (Akbarzadeh *et al* 2007). Below we illustrate how these techniques have been applied to predict reactions in the quaternary Li–B–N–H and Li–Mg–N–H systems.

5.1. Enumeration of desorption products for $Li_4BN_3H_{10}$

Several groups have recently reported the formation of a new quaternary hydride phase, $Li_4BN_3H_{10}$, capable of desorbing more than 10 wt% H_2 (Pinkerton *et al* 2005, Meisner *et al* 2006, Pinkerton *et al* 2006, Aoki *et al* 2005, Nakamori *et al* 2006b, Chater *et al* 2006, Noritake *et al* 2006). However, despite this high capacity, initial experiments suggested that the utility of this hydride for automotive applications was limited due to (a) the high temperatures ($T > 520$ K) needed to trigger hydrogen release, and (b) its apparent irreversibility (Pinkerton *et al* 2005). While it has been speculated that the difficulties encountered during rehydriding were the result of an exothermic dehydriding reaction (Pinkerton *et al* 2005), subsequent calorimetry experiments were unable to definitively determine the exothermic or endothermic nature of H_2 desorption: the calorimetry signal for hydrogen release was obscured by a simultaneous signal arising from the exothermic solidification of a (solid) reaction product(s) (Nakamori *et al* 2006b). To further complicate matters, the identity of the product phases following H_2 desorption was not well established (Pinkerton *et al* 2005, Aoki *et al* 2005, Nakamori *et al* 2006b).

Lacking fundamental thermodynamic data for $Li_4BN_3H_{10}$, it is not possible to determine whether lower desorption temperatures are possible, or whether on-board reversibility could be achieved. For example, an exothermic or weakly endothermic enthalpy (i.e., $\Delta H < \sim 20$ kJ/mol H_2) would preclude on-board reversibility. It would also indicate that the high temperatures required for desorption were the result of slow kinetics, rather than inappropriate thermodynamics, suggesting that catalysts may be useful in reducing the desorption temperature. (On the basis of thermodynamics alone, a small or negative ΔH would result in H_2 release at low temperatures.) Experiments aimed at clarifying these issues are time-consuming and costly: a trial-and-error search for suitable catalysts would be necessary to explore whether desorption temperatures could be lowered. Hence the ability to predict thermodynamics quickly and accurately via first-principles calculations would be of great value.

In order to clarify these issues, without undertaking additional and possibly futile experiments, a series of first-principles calculations were used to identify the likely $Li_4BN_3H_{10}$ desorption products and their associated thermodynamics (Siegel *et al* 2007a). As a preliminary step, we evaluated the formation enthalpy of $Li_4BN_3H_{10}$ both from the elements and via the experimentally observed 3:1 mixture of $LiNH_2$ and $LiBH_4$ (table 1). We find $Li_4BN_3H_{10}$ formation (from $LiNH_2$ and $LiBH_4$) to be exothermic, consistent with reports from the literature (Pinkerton *et al* 2005, Nakamori *et al* 2006b, Chater *et al* 2006, Herbst and Hector 2006).

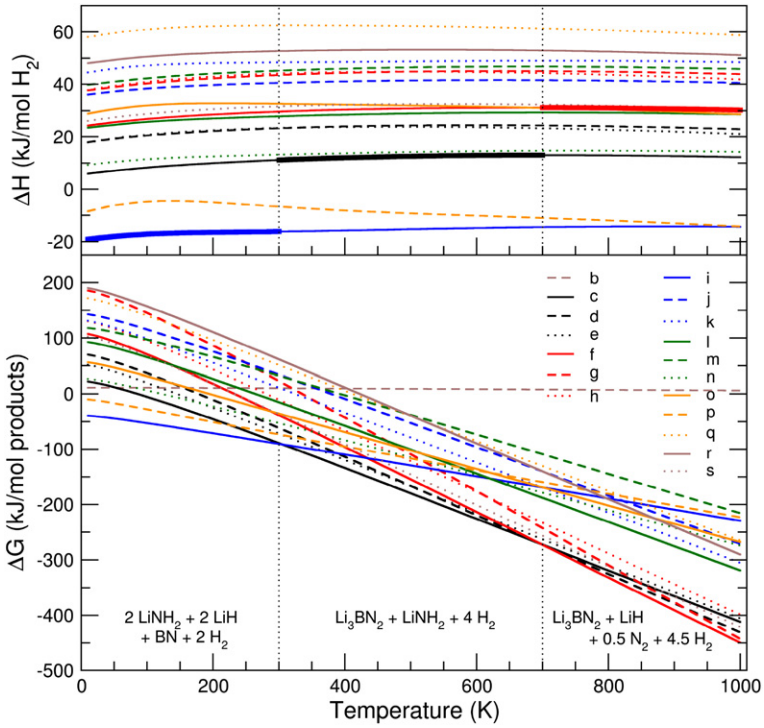

Figure 3. Calculated enthalpies (ΔH, top panel) and free energies (ΔG, bottom panel) of candidate $Li_4BN_3H_{10}$ dehydrogenation reactions as a function of temperature at $p = 1$ bar. The reactions are labeled as in table 2. Three unique sets of reaction products appear over various temperatures, and their respective ranges of stability are identified using dotted vertical lines (bottom panel). The enthalpies corresponding to these three reactions are highlighted in bold (top panel).

Table 2. Calculated reaction energies (ΔE), enthalpies (ΔH) (both in units of kJ/(mol H_2), and free energies (ΔG, in kJ/(mol products)) for candidate $Li_4BN_3H_{10}$ dehydrogenation reactions at $p = 1$ bar.

	Reaction	ΔE	$\Delta H^{T=300\ \mathrm{K}}$	$\Delta G^{T=300\ \mathrm{K}}$
(c)	$Li_4BN_3H_{10} \rightarrow Li_3BN_2 + LiNH_2 + 4H_2$	28.2	11.2	−88.8
(d)	$Li_4BN_3H_{10} \rightarrow Li_3BN_2 + 1/2Li_2NH + 1/2NH_3 + 4H_2$	40.6	23.4	−61.4
(e)	$Li_4BN_3H_{10} \rightarrow Li_3BN_2 + LiH + NH_3 + 3H_2$	42.6	23.5	−71.6
(f)	$Li_4BN_3H_{10} \rightarrow Li_3BN_2 + LiH + 1/2N_2 + 9/2H_2$	50.2	29.7	−38.2
(g)	$Li_4BN_3H_{10} \rightarrow Li_3BN_2 + Li + 1/2N_2 + 5H_2$	61.9	43.5	23.0
(h)	$Li_4BN_3H_{10} \rightarrow Li_3BN_2 + Li + NH_3 + 7/2H_2$	60.4	44.1	−10.5
(i)	$Li_4BN_3H_{10} \rightarrow 2LiNH_2 + 2LiH + BN + 2H_2$	6.4	−16.1	−90.1
(j)	$Li_4BN_3H_{10} \rightarrow LiNH_2 + Li_3N + BN + 4H_2$	56.9	40.5	34.1
(k)	$Li_4BN_3H_{10} \rightarrow 4LiH + BN + N_2 + 3H_2$	79.6	48.5	11.1
(l)	$Li_4BN_3H_{10} \rightarrow 2Li_2NH_2 + BN + 4H_2$	45.3	27.9	−14.9
(m)	$Li_4BN_3H_{10} \rightarrow 2LiNH_2 + BN + 2Li + 3H_2$	60.0	45.1	32.3
(n)	$Li_4BN_3H_{10} \rightarrow LiNH_2 + Li_2NH + LiH + BN + 3H_2$	32.3	13.2	−52.5
(o)	$Li_4BN_3H_{10} \rightarrow Li_2NH + 2LiH + BN + NH_3 + 2H_2$	55.9	32.7	−35.4
(p)	$Li_4BN_3H_{10} \rightarrow LiNH_2 + 3LiH + BN + NH_3 + H_2$	27.7	−6.6	−73.0
(q)	$Li_4BN_3H_{10} \rightarrow Li_3N + LiH + BN + NH_3 + 3H_2$	80.9	62.6	51.3
(r)	$Li_4BN_3H_{10} \rightarrow 1/2Li2NH + Li_3N + BN + 1/2NH_3 + 4H_2$	69.3	52.7	61.5
(s)	$Li_4BN_3H_{10} \rightarrow Li_3BN_2 + 1/3Li_3N + 2/3NH_3 + 4H_2$	48.7	31.7	−35.9

For $Li_4BN_3H_{10}$ desorption, seventeen unique candidate reactions were examined (Siegel *et al* 2007a) (see table 2), and for each, the reaction energies (ΔE), enthalpies, and free energies (ΔG) were evaluated. The respective enthalpies and free energies are plotted as a function of temperature in figure 3. A key result from these calculations is the existence of several reactions having negative reaction free energies ($\Delta G < 0$, see rightmost columns of table 2). In particular, reactions (i), (c), and (f) were identified as having the most negative $\Delta G'$s in three non-overlapping regions within the temperature range $T = 0$–1000 K (figure 3, bottom panel). These 3 reactions therefore represent the thermodynamically preferred decomposition products. Their composition and respective temperature ranges of stability are:

$2LiNH_2 + 2LiH + BN + 2H_2$ $(T < 300\ \mathrm{K})$
(reaction i)

$Li_3BN_2 + LiNH_2 + 4H_2$ $(300\ \mathrm{K} \leqslant T < 700\ \mathrm{K})$
(reaction c)

$Li_3BN_2 + LiH + 1/2N_2 + 9/2H_2$ $(700\ K \leqslant T)$

(reaction f).

The fact that there are several desorption reactions having $\Delta G < 0$ at low temperatures, combined with the observation that $Li_4BN_3H_{10}$ is known to exist experimentally, suggests that $Li_4BN_3H_{10}$ is a metastable phase. Indeed, for $T < 300$ K, $Li_4BN_3H_{10}$ should decompose exothermically via reaction (i) into a mixture of $2LiNH_2 + 2LiH + BN + 2H_2$.

Of the three likely reactions, only reaction (c) takes place within the temperature range where H_2 desorption has been experimentally observed (Pinkerton *et al* 2005). The calculated enthalpy for this reaction (table 2) ranges from ∼11–13 kJ/(mol H_2) for $T = 300$–500 K, indicating that H_2 release in this temperature range is a weakly endothermic process[5]. The relatively small dehydriding enthalpy is consistent with the failed re-hydriding attempts reported in the literature (Pinkerton *et al* 2005) and suggests that hydrogen release from $Li_4BN_3H_{10}$ is a kinetically—as opposed to thermodynamically—hindered process. Hence, one may reasonably expect that catalysts should prove beneficial in lowering desorption temperatures (Pinkerton *et al* 2006). However, the calculated thermodynamics reveal that on-board reversibility cannot be achieved via exposure to H_2 pressures typically envisioned for refueling ($P < 1000$ bar).

5.2. Automated linear programming approach to determining favored reaction pathways

As shown above for the case of $Li_4BN_3H_{10}$, predicting thermodynamically favored hydrogen storage reactions in multinary systems is a difficult task due to the large number of possible end products and competing reaction pathways. It is clear that this method of guessing decomposition pathways based on chemical intuition and enumeration becomes unmanageably difficult for more complex multicomponent systems. In this section, we show that the lowest free energy pathway can be predicted directly, without having to consider all possibilities or resort to (often faulty) chemical intuition. In addition, we show a few examples of reactions where chemical intuition breaks down qualitatively and can erroneously suggest that reactions are thermodynamically reasonable (Nakamori *et al* 2005a, 2005b, Alapati *et al* 2006), when our automated approach proves that in fact they are not. Furthermore, the developed theoretical framework allows us to formulate a set of simple thermodynamic guidelines (Siegel *et al* 2007b), or rules, which are universally correct and should be used to verify that proposed reaction pathways are thermodynamically reasonable.

The details of our approach to determining hydride phase diagrams are given in Akbarzadeh *et al* (2007). We start from the grand-canonical Gibbs free energy for a multi-phase solid in contact with a gas-phase reservoir of hydrogen. In particular, we consider a situation where the storage material, characterized by a certain ratio of non-hydrogen species can exchange hydrogen molecules with a reservoir of H_2 gas at a given chemical potential, $\mu_{H_2}(p, T)$, which is determined by the temperature, T, and pressure, p. Given the free energies of all possible phases in the given multicomponent hydride system, the grand-canonical Gibbs free energy is given by the following expression:

$$\Xi(T, p) = \sum_i x_i F_i(T) - \frac{\mu_{H_2}(T, p)}{2} \sum_i x_i n_i^H, \qquad (3)$$

where $F_i(T)$ is the free energy of phase 'i' (we neglect the pressure dependence of the free energies of solid phases), n_i^H is the number of hydrogen ions in one formula unit of phase 'i', and x_i are the unknown variable molar fractions of phases coexisting at a given composition, temperature, and pressure. The weight fraction of hydrogen in the solid phase varies with temperature and pressure and is determined from the minimization of the free energy with respect to the mole fractions x_i. The molar fractions are determined by minimizing equation (3), subject to the following mass-conservation constraints for non-hydrogen species:

$$f_s = \sum_i x_i n_i^s = \text{const} \qquad \text{for } \forall s \neq H, \qquad (4)$$

where n_i^s is the number of ions of type 's' in one formula unit of phase 'i', and f_s represent given molar ratios of the non-hydrogen species (i.e., Li, Mg, and N for the Li–Mg–N–H system). Following standard conventions, the latter are be normalized to obey $\sum_{s \neq H} f_s = 1$. Equations (3) and (4) constitute a linear programming problem, where the unknown variables are molar fractions of the possible phases, x_i. To obtain x_i as functions of composition, pressure, and temperature, we minimize equation (3) for a decreasing sequence of hydrogen chemical potentials $\mu_{H_2}(T, p)$, starting from $T = 0$ K, where μ_{H_2} is given by the total energy of the H_2 molecule. Since phase transformations and hydrogen release reactions manifest themselves as changes in the molar fractions x_i, reactions are identified by comparing the computed molar fractions at two successive values of the chemical potential. The reactants and reaction products are easily found by taking the difference between the two sets of x_i. In Akbarzadeh *et al* (2007), we have applied this formalism to the Li–Mg–N–H system.

Nitrogen-containing amide/imide systems emerged as promising hydrogen storage systems after Chen *et al* (2002) reported reversible extraction of H_2 from a mixture of $LiNH_2$ and LiH. Although $LiNH_2 + LiH$ can store hydrogen at high gravimetric densities, it cannot be used for on-board storage, as the temperatures required to extract H_2 are too high (above 570 K). This is because hydrogen in $LiNH_2 + LiH$ is too strongly bound, with an enthalpy of approximately 66 kJ/molH_2 (Chen *et al* 2002, Kojima and Kawai 2005). Many attempts have been made to destabilize the amide by mixing it with other hydrides, in particular MgH_2. A 2:1 mixture of $LiNH_2$ and MgH_2 has been found to be effective (Luo 2004a, 2004b, Luo and Sickafoose 2006), but reactions involving other compositions in the Li–Mg–N–H system have

[5] Although experiments report that H_2 desorption occurs from the molten $Li_4BN_3H_{10}$ state, in our calculations we approximate desorption as occurring from the solid phase. This approximation suggests that our calculated desorption enthalpy likely overestimates the enthalpy of desorption from the liquid state.

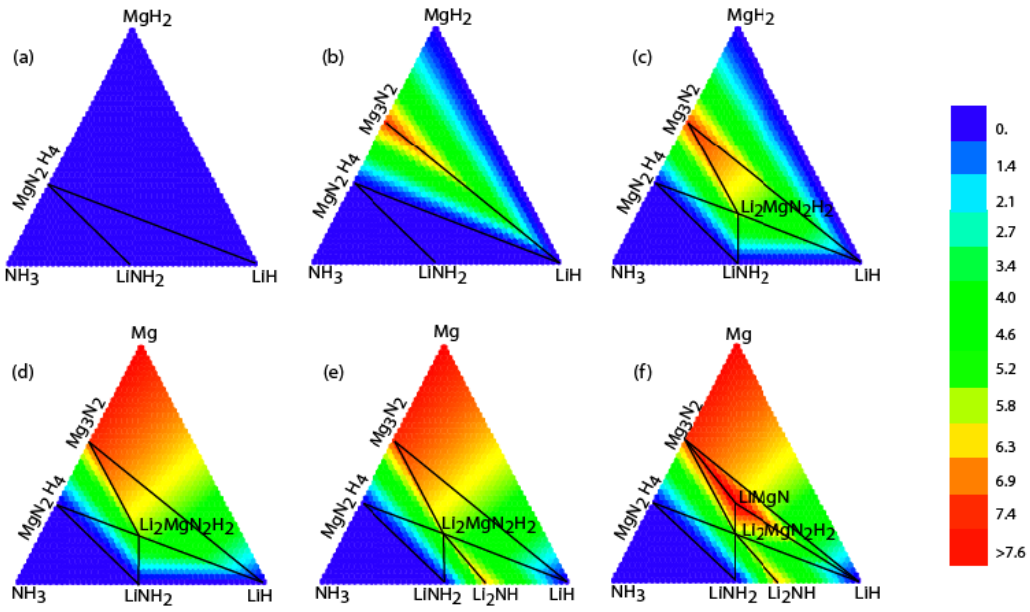

Figure 4. Calculated equilibrium phase diagrams (Gibbs triangles) for the Li–Mg–N–H system. Each diagram refers to a specific temperature range: (a) $T < 30$ K, (b) 130 K $\leqslant T <$ 426 K, (c) 426 K $\leqslant T <$ 458 K, (d) 458 K $\leqslant T <$ 606 K, (e) 606 K $\leqslant T <$ 734 K, and (f) 734 K $\leqslant T <$ 780 K. Shading indicates the amount of hydrogen released (in wt% H_2) relative to the starting mixture at $T = 0$ K.

Table 3. Predicted sequence of thermodynamically favored hydrogen storage reactions in the Li–Mg–N–H system. For each reaction, we list the amount of H_2 released, wt% H_2, calculated and experimentally measured enthalpies and entropies at $T = 500$ K, and transition temperatures at atmospheric pressure, $T_{1\ \mathrm{bar}}$ (K). References for experimental enthalpies and entropies: rxn. (ii) Luo (2004a, 2004b) and Yang *et al* (2007a); rxn. (iii) Stampfer *et al* (1959): rxn. (iv) Chen *et al* (2002) and Kojima and Kawai (2005). Two additional strongly endothermic reactions were also predicted from our computational approach (not listed) which are predicted to occur only at very high temperatures (see Akbarzadeh *et al* 2007).

No.	Reaction	Wt% H_2	$\Delta H^{T=500\ \mathrm{K}}$	ΔH^{exp}	$\Delta S^{T=500\ \mathrm{K}}$	ΔS^{exp}	$T_{1\ \mathrm{bar}}$
(i)	$Mg(NH_2)_2 + 2MgH_2 \rightarrow Mg_3N_2 + 4H_2$	7.41	15		114		130
(ii)	$2LiH + Mg(NH_2)_2 \rightarrow Li_2Mg(NH)_2 + 2H_2$	5.59	47	39 41.6	110	116	426
(iii)	$MgH_2 \rightarrow Mg + H_2$	7.67	63	74.6	137	134.8	458
(iv)	$LiH + LiNH_2 \rightarrow Li_2NH + H_2$	6.53	72	66.1 66.6	119	120	606
(v)	$2LiH + Li_2Mg(NH)_2 + Mg_3N_2 \rightarrow 4LiMgN + 2H_2$	2.18	80		109		734

also been proposed (Leng *et al* 2004, Nakamori *et al* 2005a, 2005b, Alapati *et al* 2006) and it remains unclear what is the best reversible material composition. Here, we show that, for a given chemical inventory of compounds, our method can easily predict all thermodynamically reversible H_2 storage reactions in this technologically important multicomponent system.

There are 14 compounds with known crystal structures that have Li, Mg, N, and H as their constituents. First-principles DFT calculations of the total energies and phonon dispersions for all these compounds were carried out to obtain the free energies $F_i(T)$ entering equation (3). We excluded a few known compounds (such as MgNH), which have been reported to exist, but their crystal structures are not known. We also left out metallic alloys between Li and Mg, since at practical temperatures and pressures they are expected to disproportionate into LiH and MgH_2 (or Mg). Finally, we removed molecular nitrogen from the list of compounds to inhibit the decomposition of ammonia, which is well known to be kinetically inhibited.

Figure 4 shows the calculated phase diagrams for the Li–Mg–N–H system at atmospheric pressure. To represent various ratios of Li:Mg:N, we adopt the standard Gibbs triangle convention for drawing ternary phase diagrams. As shown in figure 4(a), at temperatures below 130 K the fully hydrided system exhibits MgH_2, $Mg(NH_2)_2$, solid NH_3, $LiNH_2$, and LiH as stable compounds. Note that our results indicate that there is no equilibrium tie-line between $LiNH_2$ and MgH_2. This is in accord with experimental observations for this system: for instance, ball-milling a mixture of $LiNH_2$ and MgH_2 leads to the formation of $Mg(NH_2)_2$ and LiH, where in fact there is an equilibrium tie-line in our calculated phase diagram between the latter two phases (see figure 4(a)). The binary hydride phases MgH_2, LiH, and NH_3 occupy the vertices of the Gibbs triangle in figure 4(a), while the Mg amide and Li amide phases are represented by points on the Mg–N and Li–N edges of this triangle, respectively. Lines represent compositions where two phases coexist, while the triangular regions enclosed by these lines represent three-phase

coexistence of the phases at the vertices of these triangles. Upon increasing temperature, a sequence of reactions, given in table 3, leads to the decomposition of hydrides and appearance of new phases and phase fields in the phase diagrams, as shown in figure 4 for temperatures up to 780 K at a hydrogen pressure of 1 bar. For instance, the first reaction to occur is the decomposition of Mg amide at a low temperature of 130 K, which leads to the disappearance of $Mg(NH_2)_2$ from the phase diagram and the appearance of the decomposition product, Mg_3N_2 (see figure 4(b)). The next reaction to occur is the well-known 'Sandia reaction' given by the third row in table 3, which leads to the appearance of the mixed imide phase $Li_2Mg(NH)_2$, in the center of the Gibbs triangle in figure 4(c). It is seen from the data in table 3 that none of the thermodynamically allowed reactions in the Li–Mg–N–H system fall within the range of temperatures accessible to PEM fuel cells.

The important conclusion is that, for a given multicomponent system there is a strictly defined universal set of thermodynamically reversible reactions; this set is dictated by the types of elements involved and bulk thermodynamics of the possible compounds, and therefore cannot be easily altered. This fact is easy to understand if one remembers that, for a fixed pressure, the types of phases present are uniquely determined by minimizing equation (3), and change only at certain values of temperature where the overall balance of Gibbs energies between reaction products and reactants changes sign. Adjusting the composition of the starting material can only optimize the amount of hydrogen released within a given pressure and temperature window, and cannot be used to access qualitatively different storage reactions that are not present in this universal set, e.g. table 3. New storage reactions can only be created by adding new elements to the multicomponent mix.

It is instructive to see how chemical intuition can fail and lead to incorrect predictions for reaction pathways. For instance, in a comprehensive study of destabilization reactions, Alapati *et al* (2006) predicted that a 1:1 mixture of lithium amide and magnesium hydride could release 8.2 wt% H_2:

$$LiNH_2 + MgH_2 \leftrightarrow LiMgN + 2H_2. \quad (5)$$

Alapati *et al* calculated an enthalpy of 32 kJ/molH_2, excluding vibrational contributions, which seems to suggest that equation (5) could be a reversible, near-ambient H_2 storage reaction. Other reactions with different ratios of Li amide and Mg hydride have been proposed (see, e.g., Leng *et al* 2004, Nakamori *et al* 2005a, 2005b), which seem to suggest that new hydrogen storage reactions with improved properties might be obtained by simply tuning the molar ratios of the starting compounds in the Li–Mg–N–H system. We emphasize that this is not possible, since the possible reaction pathways in multicomponent systems are tightly constrained by bulk thermodynamics, which favors a universal set of reactions determined only by the chemical identity of the constituents. As for the proposed reaction in equation (5), instead of proceeding in one step, it happens via a series of intermediate reactions with sequentially increasing enthalpies. The linear programming approach predicts that a 1:1 mixture of $LiNH_2$ and MgH_2 will decompose as follows:

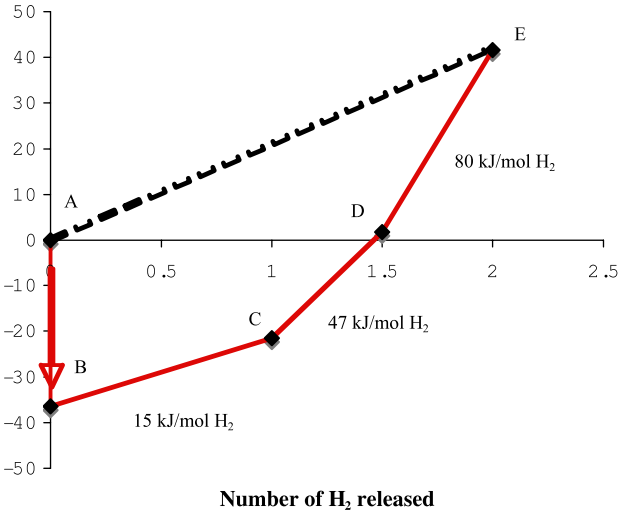

Figure 5. Predicted decomposition diagram of a reaction proposed by Alapati *et al* (2006) involving a 1:1 mixture of $LiNH_2$ and MgH_2. Our linear programming approach predicts that the reaction does not proceed according to equations (5) (A-to-E), but rather the lowest energy thermodynamic pathway consists of four steps (A-to-B, B-to-C, C-to-D, and D-to-E) which are given by equations (6)–(9), respectively.

$$LiNH_2 + MgH_2 \rightarrow LiH + \tfrac{1}{2}Mg(NH_2)_2 + \tfrac{1}{2}MgH_2 \quad (6)$$

$$\rightarrow LiH + \tfrac{1}{4}Mg(NH_2)_2 + \tfrac{1}{4}Mg_3N_2 + H_2 \quad (7)$$

$$\rightarrow \tfrac{1}{2}LiH + \tfrac{1}{4}Mg_3N_2 + \tfrac{1}{4}Li_2Mg(NH)_2 + \tfrac{3}{2}H_2 \quad (8)$$

$$\rightarrow LiMgN + 2H_2. \quad (9)$$

The scenario of these sequential reactions is shown in figure 5. First, magnesium amide will form exothermically via equation (6) without hydrogen release, corresponding to the downward arrow (A-to-B) in figure 5. In the next step, half of the MgH_2 and half of the Mg amide will form Mg_3N_2 via the endothermic reaction in equation (7), which releases H_2 with an enthalpy of 15 kJ/mol H_2; this is in fact rxn. (i) In table 3, and corresponds to the first sloping line (B-to-C) in the convex hull of figure 5 (the slope of the line connecting the reactants and the end products is the enthalpy of each reaction). The third step is the well-known reaction producing a mixed Li–Mg imide, equation (8), which is the same as rxn. (ii) in table 3 (C-to-D in figure 5). Finally, a ternary nitride is formed according to equation (9), which is the predicted rxn. (v) in table 3 (D-to-E in figure 5). The enthalpies of the 3rd and 4th steps are 47 and 80 kJ/mol H_2 at $T = 500$ K, respectively. We conclude that only the third step is close to the enthalpy range that is thermodynamically suitable for on-board storage, and this step corresponds to the well-known 'Sandia' reaction suggested by Luo (2004a, 2004b) and Luo and Sickafoose (2006). This example demonstrates that what seems like a reasonable reaction with 'good' thermodynamics (equation (5)), on closer inspection turns out to be a multi-step reaction sequence, from which only a few steps (if any) may exhibit favorable thermodynamics. An automated method, such as ours, is crucial for predicting the preferred pathway, as opposed to the currently popular practice of simply guessing the likely reactions.

6. Prediction of novel hydrogen storage reactions: thermodynamic guidelines and their application to destabilized hydride mixtures

As the preceding two sections illustrate (Siegel *et al* 2007a, Akbarzadeh *et al* 2007), the prediction of thermodynamically realistic hydrogen storage reactions in multicomponent systems is a non-trivial task (Yang *et al* 2007b, 2007c, Lewis *et al* 2007). In light of these difficulties we have developed a set of thermodynamic guidelines aimed at facilitating more robust screening of candidate reactions (Siegel *et al* 2007b). The guidelines can be applied to thermodynamic data regardless of its origin (experiment or theory), and have been used to (i) reassess the validity of reactions recently reported in the literature (Alapati *et al* 2006), and to (ii) vet a list of more than 20 candidate reactions based on destabilized $LiBH_4$ and $Ca(BH4)_2$ borohydrides (Siegel *et al* 2007b). Below we briefly discuss the guidelines, and demonstrate how they have been used to predict several new reactions having both favorable thermodynamics and relatively high hydrogen densities, ranging from 5–9 wt% H_2 to 85–100 g H_2/L.

Borohydride compounds, for example $LiBH_4$ and $Ca(BH_4)_2$, have attracted considerable interest as potential hydrogen storage materials due to their relatively high hydrogen densities (up to 18 wt% H_2 in $LiBH_4$) (Soulie *et al* 2002, Zuttel *et al* 2003, Nakamori *et al* 2006a, Lodziana *et al* 2004, Miwa *et al* 2006). Nevertheless, the practical utility of borohydrides in automotive applications is hindered by their thermodynamic stability (i.e., large desorption enthalpy), resulting in impractically high temperatures for hydrogen desorption. Based on earlier work by Reilly *et al* (1968), Vajo *et al* (2005) recently demonstrated that $LiBH_4$ could be 'destabilized' by mixing with MgH_2, due to the exothermic formation of MgB_2 as a product of the H_2 desorption reaction:

$$LiBH_4 + \tfrac{1}{2}MgH_2 \rightarrow LiH + \tfrac{1}{2}MgB_2 + 2H_2.$$

In other words, the desorption enthalpy of the $LiBH_4$–MgH_2 mixture can be decreased below those of the isolated compounds due to the formation of the boride phase. While the destabilization effect in this case was not large enough—the extrapolated temperature at which $P = 1$ bar was still too high [$T_{des} \sim 500$ K (Vajo *et al* (2005))]—the concept of destabilizing strongly bound hydrides via mixing should be generally applicable to other mixtures. Using first-principles free energy calculations we have explored whether the strongly bound compounds $LiBH_4$ and $Ca(BH_4)_2$ can be (further) destabilized by mixing with various metals and metal hydrides (Siegel *et al* 2007b). The results of these calculations comprise a list of more than 20 candidate reactions which are summarized in table 4.

As a means to introduce the thermodynamic guidelines, we draw attention to the first column of table 4, and in particular to the reactions identified with asterisks (*). These reactions are noteworthy in that they illustrate the difficulties that may arise when attempting to 'guess' at reactions. For example, all of the candidate reactions are written as simple, single-step reactions. While this may seem reasonable given the mechanism proposed in Vajo *et al* (2005) as we discuss below, some of these reactions should proceed via multiple-step pathways, with each step having thermodynamic properties that are distinct from the presumed single-step pathway.

We group the examples of how chemical intuition might fail into three categories, and for each class, give a general guideline describing the thermodynamic restriction:

(1) *Reactant mixtures involving 'weakly bound' compounds*. We refer here to systems where the enthalpy to decompose one (or more) of the reactant phases is less than the enthalpy of the proposed destabilized reaction; thus, the weakly bound phase(s) will decompose before (i.e., at a temperature below that which) the destabilized reaction can proceed. Two examples of this behavior can be found in table 4. The first case pertains to reactions 13–16, which, based on their larger enthalpies relative to reaction 12, would appear to 'stabilize' $Ca(BH_4)_2$. In reality, $Ca(BH_4)_2$ will decompose before any of the higher temperature reactions 13–16 will occur, indicating that it is impossible to stabilize a reaction in this manner. Additional examples of this scenario occur in reactions 1, 8, 17, and 21, which involve the metastable AlH_3 and CrH_2 phases. In the case of reaction 1, AlH_3 will decompose first (yielding Al and 3/2 H_2), followed by reaction of Al with $LiBH_4$ (reaction 2). The consequences of this behavior are significant, since although the intended reaction 1 has an enthalpy (~40 kJ/mol H_2)—which falls within the $\Delta H = 20$–50 kJ/mol H_2 range targeted for fuel cell applications—in reality the reaction will consist of two steps, the first of which has an enthalpy below the targeted range (AlH_3 decomposition), while the second (reaction 2) has an enthalpy above this range. *Guideline 1: the enthalpy of the proposed destabilized reaction must be less than the decomposition enthalpies of the individual reactant phases*.

(2) *Unstable combinations of product or reactant phases*. Reaction 4 illustrates how the seemingly straightforward process of identifying stable reactant and product phases can become unexpectedly complex. Here, the starting mixture of $LiBH_4$ and Mg is unstable and will undergo the exothermic solid-state transformation:

$$2LiBH_4 + Mg \rightarrow \tfrac{3}{2}LiBH_4 + \tfrac{3}{4}MgH_2 + \tfrac{1}{4}MgB_2 + \tfrac{1}{2}LiH.$$

The exothermic nature of reaction can be understood by noting that the enthalpy of reaction 4 (46.4 kJ/mol H_2) is lower than the decomposition enthalpy of MgH_2, given by reaction 27 (62.3 kJ/mol H_2). Therefore, the total energy can be lowered by transferring hydrogen to the more strongly bound MgH_2 compound. *Guideline 2: if the proposed reaction involves a reactant that can absorb hydrogen (such as an elemental metal), the formation enthalpy of the corresponding hydride cannot be greater in magnitude than the enthalpy of the destabilized reaction*.

(3) *Adjusting molar fractions of reactants*. Reaction 3, involving a 4:1 mixture of $LiBH_4$:MgH_2, as well as the related reaction involving a 7:1 stoichiometry, $7LiBH_4 + MgH_2 \rightarrow MgB_7 + 7LiH + 11.5H_2$, were recently suggested by

Table 4. H_2 densities and calculated thermodynamics quantities for candidate H_2 storage reactions. Units are J/(K mol H_2) for ΔS_{vib} and kJ/mol H_2 for ΔE and ΔH; column 7 refers to the temperature at which $p = 1$ bar. Reactions denoted with a * will not proceed as written (see text for explanation). The enthalpies of reactions 24–27 have been measured in prior experiments, and are included here (in parentheses) to validate the accuracy of our calculations.

Rxn. No.	Reaction	Wt% (kgH_2/kg)	Vol. density (g H_2/L)	ΔE	$\Delta H^{T=300\ K}$	T, P = 1 bar (°C)	$\Delta S_{vib}^{T=300\ K}$
1*	$4LiBH_4 + 2AlH_3 \rightarrow 2AlB_2 + 4LiH + 9H_2$	12.4	106	54.8	39.6	83	−18.4
2	$2LiBH_4 + Al \rightarrow AlB_2 + 2LiH + 3H_2$	8.6	80	77.0	57.9	277	−26.9
3*	$4LiBH_4 + MgH_2 \rightarrow MgB_4 + 4LiH + 7H_2$	12.4	95	68.2	51.8	206	−23.3
4*	$2LiBH_4 + Mg \rightarrow MgB_2 + 2LiH + 3H_2$	8.9	76	65.9	46.4	170	−29.4
5	$2LiBH_4 + TiH_2 \rightarrow TiB_2 + 2LiH + 4H_2$	8.6	103	21.4	4.5		−23.3
6	$2LiBH_4 + VH_2 \rightarrow VB_2 + 2LiH + 4H_2$	8.4	105	24.7	7.2	−238	−21.7
7	$2LiBH_4 + ScH_2 \rightarrow ScB_2 + 2LiH + 4H_2$	8.9	99	48.8	32.6	26	−21.4
8*	$2LiBH_4 + CrH_2 \rightarrow CrB_2 + 2LiH + 4H_2$	8.3	109	33.9	16.4	−135	−19.2
9*	$2LiBH_4 + 2Fe \rightarrow 2FeB + 2LiH + 3H_2$	3.9	76	32.7	12.8	−163	−24.6
10	$2LiBH_4 + 4Fe \rightarrow 2Fe_2B + 2LiH + 3H_2$	2.3	65	21.6	1.2		−24.4
11	$2LiBH_4 + Cr \rightarrow CrB_2 + 2LiH + 3H_2$	6.3	84	50.9	31.7	25	−23.8
12	$Ca(BH_4)_2 \rightarrow \frac{2}{3}CaH_2 + \frac{1}{3}CaB_6 + \frac{10}{3}H_2$	9.6	107	57.1	41.4	88	−16.0
13*	$Ca(BH_4)_2 + MgH_2 \rightarrow CaH_2 + MgB_2 + 4H_2$	8.4	99	61.6	47.0	135	−16.2
14*	$2Ca(BH_4)_2 + MgH_2 \rightarrow 2CaH_2 + MgB_4 + 7H_2$	8.5	98	63.6	47.9	147	−17.0
15*	$Ca(BH_4)_2 + Mg \rightarrow CaH_2 + MgB_2 + 3H_2$	6.4	79	60.6	41.9	111	−22.0
16*	$Ca(BH_4)_2 + Al \rightarrow CaH_2 + AlB_2 + 3H_2$	6.3	83	71.7	53.4	200	−19.5
17*	$Ca(BH_4)_2 + AlH_3 \rightarrow CaH_2 + AlB_2 + \frac{9}{2}H_2$	9.1	109	51.2	36.6	39	−13.5
18	$Ca(BH_4)_2 + ScH_2 \rightarrow CaH_2 + ScB_2 + 4H_2$	6.9	102	44.8	29.2	−20	−15.9
19	$Ca(BH_4)_2 + TiH_2 \rightarrow CaH_2 + TiB_2 + 4H_2$	6.7	106	17.4	1.1		−17.7
20	$Ca(BH_4)_2 + VH_2 \rightarrow CaH_2 + VB_2 + 4H_2$	6.6	108	20.8	3.8		−16.2
21*	$Ca(BH_4)_2 + CrH_2 \rightarrow CaH_2 + CrB_2 + 4H_2$	6.5	113	29.9	13.1	−180	−13.6
22	$Ca(BH_4)_2 + Cr \rightarrow CaH_2 + CrB_2 + 3H_2$	5.0	86	45.6	27.2	−38	−16.4
23	$6LiBH_4 + CaH_2 \rightarrow CaB_6 + 6LiH + 10H_2$	11.7	93	61.9 (63)[a]	45.4	146	−22.7
24	$2LiBH_4 + MgH_2 \rightarrow MgB_2 + 2LiH + 4H_2$	11.6	96	65.6	50.4 (41)[b]	186	−21.7
25	$2LiBH_4 \rightarrow +2LiH + 2B + 3H_2$	13.9	93	81.4	62.8 (67)[b]	322	−27.1
26	$LiBH_4 \rightarrow Li + B + 2H_2$	18.5	124	103.5	89.7 (95)[c]	485	−15.3
27	$MgH_2 \rightarrow MgH + H_2$	7.7	109	64.5	62.3 (65.8–75.2)[d]	195	1.3

[a] Alapati *et al* (2006).
[b] Vajo *et al* (2005).
[c] Chase (1998).
[d] Manchester (2000).

Alapati *et al* (2006) which considered only a single-step mechanism resulting in the formation of MgB_4 and MgB_7, respectively. Here we demonstrate that these reactions will not proceed as suggested due to the presence of intermediate stages with lower energies. In fact, both hypothetical reactions have larger enthalpies ($\Delta E = 69$ (4:1) and 74 (7:1) kJ/molH_2 (Alapati *et al* 2006)) than the 2:1 mixture (reaction 24), suggesting that, upon increasing temperature, the 4:1 and 7:1 mixtures will follow a pathway whose initial reaction step is the 2:1 reaction (reaction 24), which will consume all available MgH_2. Subsequent reactions between unreacted $LiBH_4$ and newly formed MgB_2 will become thermodynamically feasible at temperatures above that of reaction 24, since their enthalpies exceed 50 kJ/mol H_2. (Similar behavior is expected for reactions 9 & 10, as the 1:1 mixture of $LiBH_4$:Fe (reaction 9) will initially react in a 1:2 ratio (reaction 10), which has a lower enthalpy.) *Guideline 3: in general, it is not possible to tune the thermodynamics of destabilized reactions by adjusting the molar fractions of the reactants. There is only one stoichiometry corresponding to a single-step reaction with the lowest possible enthalpy; all other stoichiometries will release* H_2 *in multi-step reactions, where the initial reaction is given by the lowest enthalpy reaction*[6].

In total, the preceding examples reveal that great care must be taken in predicting hydrogen storage reactions. Having ruled out the specious reactions, we now discuss the thermodynamics of the remaining reactions in table 4. Using the calculated thermodynamic data (table 4) as input to the van't Hoff equation, figure 6 plots the equilibrium H_2 desorption pressures of these reactions as a function of temperature. Included in the plot is a rectangle delineating desirable temperature and pressure ranges for H_2 storage: −40 to 100 °C, and 1–700 bar.

Our van't Hoff plot confirms that, as expected, the experimental reactions having large dehydrogenation enthalpies (reactions 24–27) yield low H_2 pressures, even at elevated temperatures. On the other hand, some of the candidate reactions, for example 5 and 19, readily evolve H_2 at very low temperatures, consistent with their low

[6] This discussion assumes that the entropies of all competing reaction pathways are similar. Our results in table 3 show that this is generally not the case; generalization of the above guidelines to the free energies is straightforward and will be presented elsewhere.

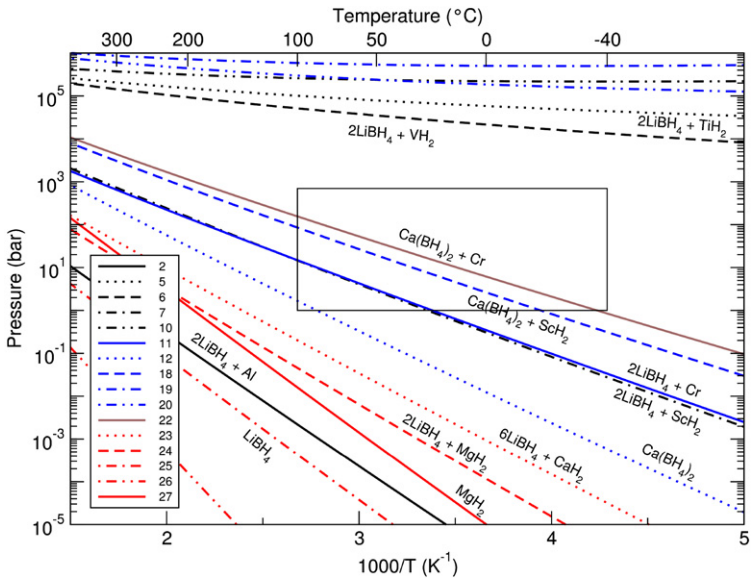

Figure 6. Calculated van't Hoff plot for reactions listed in table 4. The region within the box corresponds to desirable temperatures and pressures for on-board hydrogen storage: $p = 1$–700 bar, $T = -40$–100 °C.

enthalpies, and are therefore too weakly bound for practical, reversible on-board storage. However, four of the candidate reactions involving mixtures with ScH_2 and Cr (reactions 7 and 18; 11 and 22, respectively) desorb H_2 in pressure–temperature regimes that strongly intersect the window of desirable operating conditions. (We note that Alapati *et al* (2007) also reported reaction 7.) These reactions have room temperature enthalpies in the range of 27–33 kJ/mol H_2, relatively high H_2 densities (5–8.9 wt% H_2 and 85–100 g H_2 L^{-1}), and achieve H_2 pressures of ∼1 bar at moderate temperatures ranging from −38 to 26°C.

Thus, via a first-principles screening of a large number of candidate reactions, and the careful use of thermodynamic considerations to eliminate unstable or multi-step reactions, we predict here several reactions with attributes that surpass the state-of-the-art for reversible, low temperature storage materials.

To summarize this section, using first-principles free energy calculations we have demonstrated that further significant destabilization of the strongly bound $LiBH_4$ and $Ca(BH_4)_2$ borohydrides is possible, and we identify several high H_2-density reactions having thermodynamics compatible with the operating conditions of mobile H_2-storage applications. Unlike other recent predictions, the proposed reactions utilize only known compounds with established synthesis routes, and can therefore be subjected to immediate experimental testing. In addition, we provide guidance to subsequent efforts aimed at predicting new H_2 storage materials by illustrating common pitfalls that arise when attempting to 'guess' at reaction mechanisms (Alapati *et al* 2006), and by suggesting a set of thermodynamic guidelines to facilitate more robust predictions.

7. Conclusions

First-principles density-functional calculations, while previously a tool only for the theoretical physicist, can now be broadly applied to several areas of materials research, many of which have direct relevance to industry. Further evidence of the value of this approach can be found in our recent efforts aimed at the discovery of new hydrogen storage materials. At present, no known material exhibits the combination of high hydrogen densities, low desorption temperatures, fast kinetics, and low cost needed for automotive applications. New hydrides with enhanced properties must be developed.

Toward these ends, in this review we have illustrated how first-principles computation can accelerate the search for new hydrogen storage materials. To be effective this approach must successfully address (at least) three computational challenges: (i) accurate prediction of decomposition thermodynamics, (ii) prediction of crystal structures for new hydrides, and (iii), prediction of preferred decomposition pathways. We have demonstrated the significance of each of these challenges through several examples:

(i) For decomposition thermodynamics, we show that the GGA generally gives reasonably accurate enthalpies compared to experimentally measured values across a series of metal hydrides. Vibrational contributions to the enthalpy improve agreement between theory and experiment to within ∼15 kJ/mol H_2, compared to ∼19 kJ/mol without. While further gains in computational accuracy—perhaps via improved exchange–correlation functionals—would certainly be welcome, the present DFT-GGA approach is clearly sufficient to distinguish thermodynamically promising materials from those likely to be a thermodynamic 'dead end'.

(ii) Next, database searching and lattice algebra enumeration were presented as two examples of methods for determining ground state crystal structures of new hydrides. These methods provide a crucial capability, since the accuracy of any first-principles thermodynamic prediction will be impacted by the crystal structures of the phases in question. Although both methods were shown

to be successful in identifying low energy phases, more research in this area is highly desirable, especially in cases where (for example) the database of candidate structure prototypes is limited.

(iii) Finally, we presented two techniques for elucidating thermodynamically preferred reaction pathways: pathway enumeration and an automated, phase diagram approach based on linear programming. Pathway enumeration, illustrated for the case of $Li_4BN_3H_{10}$ decomposition, is a brute-force approach wherein one seeks to identify the preferred pathway by enumerating all possible reactions and products. A more comprehensive and efficient alternative to enumeration was presented in the form of an automated, phase diagram approach. This new method *automatically* identifies *all* thermodynamically allowed reactions occurring within a prescribed composition–temperature–pressure space, and largely eliminates the guesswork associated with predicting reactions. The approach has been used to reassess several reactions reported in the literature for the Li–Mg–N–H system, and has motivated the development of a set of 'thermodynamic guidelines' meant to facilitate more robust predictions of hydrogen storage reactions.

In total, these capabilities establish first-principles computation as an invaluable resource in predicting the thermodynamics of hydrogen storage reactions. However, despite these capabilities, it is important to recognize that favorable thermodynamics is a *necessary, but not sufficient* condition for the development of suitable hydrogen storage materials. Although not discussed in detail here, the *kinetics* of hydrogen uptake/release will also play a crucial role, and must be considered in any complete treatment of hydrogen storage. Since experimental identification of the rate-limiting steps in a given storage reaction remains a formidable challenge, a concerted effort to tackle the 'kinetics problem' via first-principles computation must be developed. Thus a means for both understanding and improving the kinetics of hydrogen storage may be considered as a 4th—and as-of-yet unresolved–challenge to computation.

Acknowledgments

AA and VO acknowledge financial support from the US Department of Energy under grant DE-FG02-05ER46253. CW and VO acknowledge financial support from the US Department of Energy under grant DE-FG02-07ER46433 and from the National Science Foundation under grant CBET-0730929.

References

Akbarzadeh A R, Ozoliņš V and Wolverton C 2007 *Adv. Mater.* **19** 3233
Alapati S V, Johnson J K and Sholl D S 2006 *J. Phys. Chem.* B **110** 8769
Alapati S V, Johnson J K and Sholl D S 2007 *Phys. Chem. Chem. Phys.* **9** 1438
Aoki M, Miwa K, Noritake T, Kitahara G, Makamori Y, Orimo S and Towata S 2005 *Appl. Phys.* A **80** 1409
Balogh M P, Jones C Y, Herbst J F, Hector L G and Kundrat M 2006 *J. Alloys Compounds* **420** 326
Blöchl P E 1994 *Phys. Rev.* B **50** 17953
Chase M W Jr 1998 *NIST-JANAF Thermochemical Tables* 4th edn (Washington, DC: American Chemical Society)
Chater P A, David W I F, Johnson S R, Edwards P P and Anderson P A 2006 *Chem. Commun.* **23** 2439
Chen P, Xiong Z, Luo J, Lin J and Tan K L 2002 *Nature* **420** 302
Fichtner M, Frommen C and Fuhr O 2005 *Inorg. Chem.* **44** 3479
Glass C W, Oganov A R and Hansen N 2006 *Comput. Phys. Commun.* **175** 713
Hector L G *et al* 2007 *Phys. Rev.* B **76** 014121
Hellenbrandt M 2004 *Cryst. Rev.* **10** 17
Herbst J F and Hector L G Jr 2005 *Phys. Rev.* B **72** 125120
Herbst J F and Hector L G Jr 2006 *Appl. Phys. Lett.* **88** 231904
Hohenberg P and Kohn W 1964 *Phys. Rev.* **136** B864
Juza R and Opp K 1951 *Z. Anorg. Allg. Chem.* **266** 325
Ke X Z, Kuwabara A and Tanaka I 2005 *Phys. Rev.* B **71** 184107
Kohn W and Sham L J 1965 *Phys. Rev.* **140** A1133
Kojima Y and Kawai Y 2005 *J. Alloys Compounds* **395** 236
Kresse G 1993 *Thesis* Technische Universität Wien
Kresse G and Furthmüller J 1996a *Comput. Mater. Sci.* **6** 15
Kresse G and Furthmüller J 1996b *Phys. Rev.* B **54** 11169
Kresse G and Hafner J 1993 *Phys. Rev.* B **47** 558
Kresse G and Hafner J 1994 *J. Phys.: Condens. Matter* **6** 8245
Leng H Y, Ichikawa T, Hino S, Hanada N, Isobe S and Fujii H 2004 *J. Phys. Chem.* B **108** 8763
Lewis G J, Sachtler J W A, Low J J, Lesch D A, Faheem S A, Dosek P M, Knight L M, Jensen C M, Yang J, Sudik A, Siegel D J, Wolverton C, Ozolins V and Zhang S 2007 *J. Alloys Compounds* **446/447** 355
Lodziana Z *et al* 2004 *Phys. Rev. Lett.* **93** 145501
Løvvik O M 2005 *Phys. Rev.* B **71** 144111
Løvvik O M and Swang O 2004 *Europhys. Lett.* **67** 607
Luo W 2004a *J. Alloys Compounds* **381** 284
Luo W 2004b *J. Alloys Compounds* **385** 316
Luo W and Sickafoose S 2006 *J. Alloys Compounds* **407** 274
Magyari-Kope B, Ozoliņš V and Wolverton C 2006 *Phys. Rev.* B **73** 220101
Mamatha M, Bogdanovic B, Felderhoff M, Pommerin A, Schmidt W, Schuth F and Weidenthaler C 2006 *J. Alloys Compounds* **407** 78
Manchester F D 2000 *Phase Diagrams of Binary Hydrogen Alloys* (Materials Park, OH: ASM)
Meisner G P, Scullin M L, Balogh M P, Pinkerton F E and Meyer M S 2006 *J. Phys. Chem.* B **110** 4186
Miwa K, Aoki M, Noritake T, Ohba N, Nakamori Y, Towata S I, Zuttel A and Orimo S I 2006 *Phys. Rev.* B **74** 155122
Mueller T and Ceder G 2006 *Phys. Rev.* B **74** 134104
Nakamori Y, Kitahara G, Miwa K, Towata S and Orimo S 2005b *Appl. Phys.* A **80** 1
Nakamori Y, Ninomiya A, Kitahara G, Aoki M, Noritake T, Miwa K, Kojima Y and Orimo S 2006b *J. Power Sources* **155** 447
Nakamori Y *et al* 2005a *J. Alloys Compounds* **404** 396
Nakamori Y *et al* 2006a *Phys. Rev.* B **74** 045126
Noritake T, Aoki M, Towata S, Ninomiya A, Nakamori Y and Orimo S 2006 *Appl. Phys.* A **83** 277
Noritake T, Nozaki H, Aoki M, Towata S, Kitahara G, Nakamori Y and Orimo S 2005 *J. Alloys Compounds* **393** 264
Ohoyama K, Nakamori Y, Orimo S and Yamada K 2005 *J. Phys. Soc. Japan.* **74** 483
Ozoliņš V, Majzoub E and Wolverton C 2007 unpublished
Ozoliņš V, Wolverton C and Zunger A 1998 *Phys. Rev.* B **57** 6427
Perdew J and Wang Y 1992 *Phys. Rev.* B **45** 13244
Pinkerton F E, Meisner G P, Meyer M S, Balogh M P and Kundrat M D 2005 *J. Phys. Chem.* B **109** 6
Pinkerton F E, Meyer M S, Meisner G P and Balogh M P 2006 *J. Phys. Chem.* B **110** 7967
Reilly J J and Wiswall R H 1968 *Inorg. Chem.* **7** 2254

Satyapal S, Petrovic J, Read C, Thomas G and Ordaz G 2007 *Cat. Today* **120** 246
Siegel D J, Wolverton C and Ozoliņš V 2007a *Phys. Rev.* B **75** 014101
Siegel D J, Wolverton C and Ozolins V 2007b *Phys. Rev.* B **76** 134102
Soulie J-P *et al* 2002 *J. Alloys Compounds* **346** 200
Stampfer J F, Holley C F and Suttle J F 1959 *J. Am. Chem. Soc.* **81** 3504
Vajeeston P, Ravindran P, Kjekshus A and Fjellvåg H 2004 *J. Alloy Compound* **363** L7
Vajo J J, Skeith S L and Mertens F 2005 *J. Phys. Chem.* B **109** 3719
Vanderbilt D 1990 *Phys. Rev.* B **41** 7892
Wei S and Chou M Y 1992 *Phys. Rev. Lett.* **69** 2799
Weidenthaler C, Frankcombe T J and Felderhoff M 2006 *Inorg. Chem.* **45** 3849
Wolverton C and Ozoliņš V 2007 *Phys. Rev.* B **75** 064101
Wolverton C, Ozoliņš V and Asta M 2004 *Phys. Rev.* B **69** 144109
Yang J, Sudik A and Wolverton C 2007a *J. Alloys Compounds* **430** 334
Yang J *et al* 2007b *J. Alloys Compounds* **446/447** 345
Yang J *et al* 2007c *Angew. Chem. Int. Edn* at press
Zhong Y, Wolverton C, Chang Y A and Liu Z-K 2004 *Acta Mater.* **52** 2739
Zuttel A *et al* 2003 *J. Alloys Compounds* **356/357** 515